Applied Physics Letters

Adaptable single molecule localization microscopy (aSMLM) for superresolution optical fluorescence imaging

Cite as: Appl. Phys. Lett. **119**, 173703 (2021); https://doi.org/10.1063/5.0071515
Submitted: 15 September 2021 • Accepted: 13 October 2021 • Published Online: 26 October 2021

Prakash Joshi, Aravinth S and Partha Pratim Mondal

Applied Physics Letters ARTICLE scitation.org/journal/apl

Adaptable single molecule localization microscopy (aSMLM) for superresolution optical fluorescence imaging

Cite as: Appl. Phys. Lett. **119**, 173703 (2021); doi: 10.1063/5.0071515
Submitted: 15 September 2021 · Accepted: 13 October 2021 ·
Published Online: 26 October 2021

Prakash Joshi,[1] Aravinth S,[1] and Partha Pratim Mondal[1,2,a)]

AFFILIATIONS

[1]Department of Instrumentation and Applied Physics, Indian Institute of Science, Bangalore 560012, India
[2]Applied Photonics Initiative, Indian Institute of Science, Bangalore 560012, India

[a)]Author to whom correspondence should be addressed: partha@iisc.ac.in

ABSTRACT

Single-molecule imaging over a large area is beneficial for understanding interlinked intracellular biophysical processes and cell–cell interaction. To study, the interrogation system requires real-time adaptability of the field-of-view (FOV). We developed a widefield non-scanning system (aSMLM) that consists of an autotunable illumination system. The 4*f*-autotunable optical sub-system (combination of autotunable lens and objective lens) is introduced in the illumination path to enable change of focus at the specimen plane (located at the working distance of the objective lens). The combined incident parallel beam (of wavelengths, 405 and 561 nm) is converged/diverged by the 4*f* sub-system, resulting in a change of focal spot at the working distance. The spot is essentially a defocussed field with an order increase in FOV (14.79 to 316.31 μm^2) and demonstrates better field homogeneity. However, the most important point is the tunability of the FOV in this range. A dedicated control unit is engaged to facilitate a rapid shift of focus (at a rate of 200 Hz), resulting in desirable spot-size (FOV). However, the detection subsystem is a 4*f*-system that collects light emerging from the specimen plane (located at the working distance of objective lens) and produces an image at the focus of tube-lens. The technique is further explored to study single-molecule (Dendra2-HA) clusters in transfected NIH3T3 cells that demonstrate its efficiency over a variable FOV. A near-uniform illumination of desired FOV is achieved along with a threefold increase in the number of detected single molecules. We anticipate that the proposed aSMLM technique may find immediate application in the emerging field of single-molecule biophysics and fluorescence microscopy.

The last decade has seen a lot of excitement in single molecule optical fluorescence microscopy. The ability to visualize biophysical processes in a cellular system and to discern resolution down to single molecule is incredible. Over the last decade, numerous advancements are made both at a single cell level and in multicellular organisms.[1,2] These studies include STORM/fPALM/PALM imaging in plant system to visualize cortical microtubule arrangement in Arabidopsis roots,[3] microfibril organization in onion cells,[4] influenza A virus (IAV) structural proteins during viral infection,[5–7] and understanding protein dynamics in cellular system.[8,9] Single molecule localization microscopy (SMLM) is finding numerous application in diverse research disciplines ranging from nanophysics to applied biophysics.

Biological processes are known to occur at molecular level, and the inability of traditional microscopy techniques has limited its use. The lower bound on the resolution dictated by classical physics has somewhat ceased the progress of optical microscopes and mostly provided ensemble information. This has started to change with the advent of super-resolution microscopes such as STED,[10] fPALM,[11] STORM,[12] PALM,[13] structured illumination SIM,[14] GSDIM,[15] SOFI,[16] PAINT,[17,18] SMILE,[19,20] MINFLUX,[21] and others techniques.[22–30] The availability of computational techniques has further expanded the reach of these sophisticated imaging systems.[31–34] Few techniques, such as POSSIBLE[1] and MINFLUX,[21] have even demonstrated resolution below sub-10 nm regime, and SMILE has facilitated three-dimensional imaging.[19,20] While these techniques have advanced SMLM, very little is done as far as field homogeneity and field-of-view (FOV) are concerned.

In general, SMLM involves acquiring several single molecule images, which are then localized, and relevant parameters (such as centroid and localization precision) are determined. Often the studies

are limited to localized regions and, thus, lack large area study primarily due to small FOV and poor field homogeneity. As such, the study of cellular processes at large FOV is a daunting task and has several benefits including quantization of protein distribution, characterized by biophysical parameters, such as cluster density, cluster size, and number of molecules per cluster. Some of the techniques currently used for large FOV imaging include Fourier ptychographic microscopy,[35] coupled phase and fluorescence imaging using macrolens,[36] large FOV super-resolution imaging using fiber combiner that delivers very high intensity,[37] multiregion multifocal confocal fluorescence microscope,[38] and large FOV imaging using low-magnification objective.[39] Single molecule nanoscale imaging over a large field-of-view and with a good field homogeneity is crucial for observing dynamics in live cells. Recent advances have demonstrated chip-based nanoscopy with the ability to image large areas with a lateral resolution of about 75 nm.[40] In another approach, TIRF-based imaging with flattop-like excitation profile over a large field-of-view is achieved.[41] In a similar line, Ellesfen *et al.* have demonstrated a TIRF-based imaging of local Ca^{2+} transients and redistribution of proteins in cell plasma membrane.[42] All these advances show the ability of imaging large areas and open up new avenues with application in cell and disease biology. Here, we report the tunability of the FOV. Although these techniques are useful, they are either complex or not suitable for super-resolution predominantly due to high power requirement, low resolution, and are suited for specific application. Another important aspect is the homogeneity of light field at the working distance of the objective lens. As a natural choice, most of the existing SMLM techniques use laser light source, which are Gaussian in nature. This results in non-uniform distribution of incident light, leading to large activation of single-molecules at the central region when compared to peripheral region of the beam. Thus, uniformity and homogeneity of incident field play critical role in determining the true distribution of target single molecules.

In this Letter, we propose and demonstrate a new technique (aSMLM) that can adaptively change FOV at a rapid rate. This comes with the benefit of better field homogeneity. The technique uses a special optical element called electrically controlled auto-tunable lens that can change focal-length at a fast rate (200 *Hz*). When used in conjugation with the objective lens, it is equivalent to a 4*f*-system in the illumination path, which can be used to adaptively change illumination area (FOV) at the specimen plane.

The optical setup of proposed adaptable single molecule localization microscopy (aSMLM) is shown in Fig. 1. Two independent coherent light sources of wavelength 405 and 561 nm are used for activating and exciting the photoactivable probe (present in the specimen). Two separate intensity controllers are used to deliver appropriate power to the specimen. The beams are combined using a beam-combiner BC and directed to an autotunable 4*f*-system (comprising auto-tunable lens and objective lens) by the mirror M2. A dedicated control unit CU is used to selectively choose the current for changing the aperture of autotunable lens (ATL) (optotune, Edmund Optics, SG) at a rate of 200 Hz. This alters the convergence angle of incident beam at the back-aperture of objective lens (OBJ), thereby resulting in a shift of focus and size of illumination area (FOV) at the working distance. The specimen plane (at the working distance of objective lens) is illuminated by a defocussed beam. It may be noted that the beam intensity is discussed at off-focal planes and displays a better field homogeneity over the FOV when compared to a focused Gaussian beam (used in traditional SMLM) that leads to field inhomogeneity. This is clear from the schematic diagram shown in the inset figure (see Fig. 1), where the FOV of convergent beam (green rays) is larger at working distance (WD) of objective lens when compared to the parallel beam (black rays). The detection system is essentially a 4f-system (comprising objective lens and tube lens), for which the object plane is at the working distance of the objective lens, and the image forms at focus of tube-lens. The objective lens (OBJ) collects fluorescence from the defocussed plane and directed it to the camera (D) by the mirror (M3). On its way, the image is magnified two times by the magnifying optics (MO), and the beam passes through a series of optical filters [low-pass

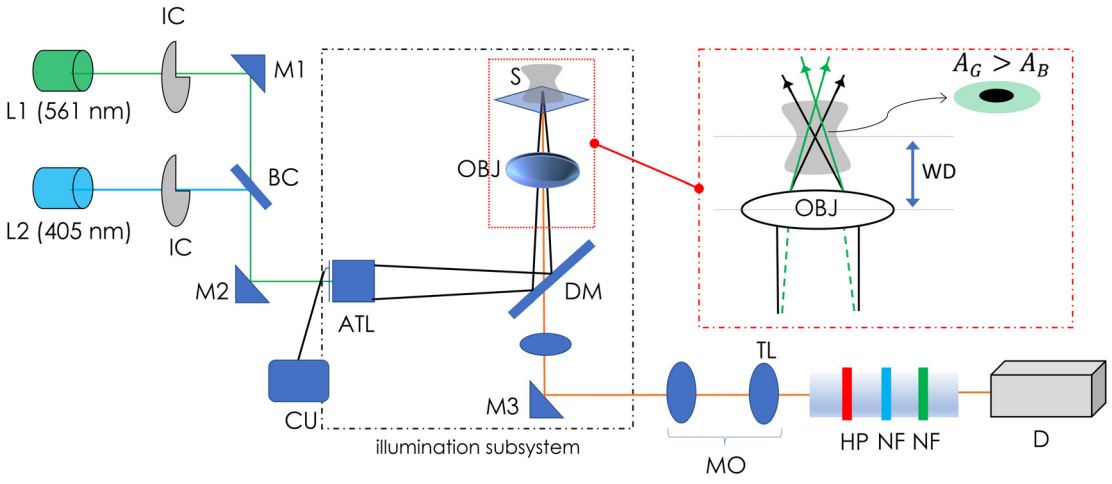

FIG. 1. Schematic diagram of the proposed aSMLM optical system (lasers: L1 and L2; intensity controller: IC; mirrors: M1, M2, and M3; beam combiner: BC; autotunable lens: ATL; control unit: CU; dichroic mirror: DM; objective: OBJ; sample: S; magnifying optics: MO; tube-lens: TL; high-pass filter: HP; notch filter: NF; detector: D). An auto-tunable 4*f* optical sub-system (combination of autotunable lens and objective lens) is used to adaptably change the FOV at the working distance of objective lens. The detection system is a fluorescence-based widefield detection with a 2*X* magnification.

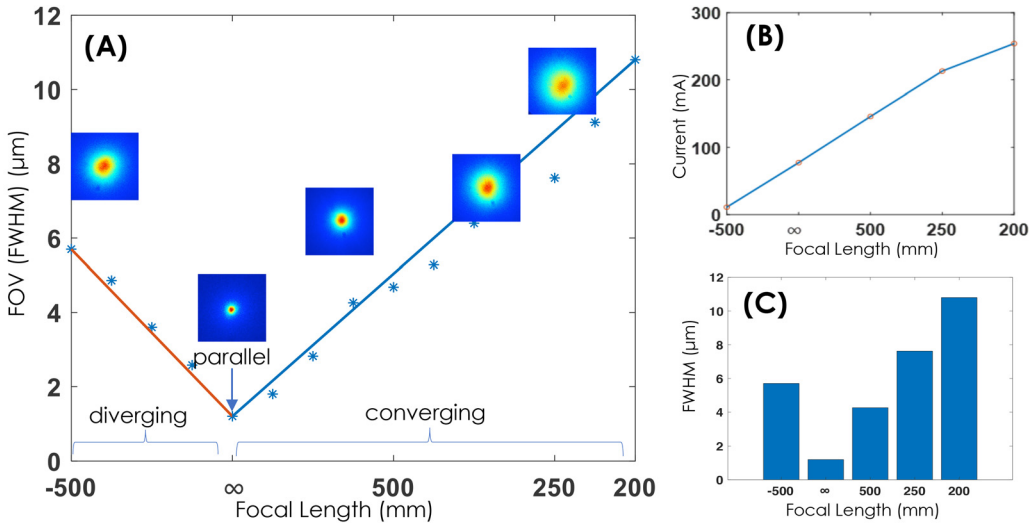

FIG. 2. (a) The scaling of FOV at varying focal lengths of ATL. [(b), (c)] The corresponding variation of focal length with current and the FOV-histogram.

filters (LPs) and notch-filters (NFs) for 405 and 561 nm light, respectively] to allow only the fluorescence from the specimen.

Figure 2(a) shows the variation in FOV with the focal length of the auto-tunable lens along with the beam size (see inset). The field is recorded by placing fluorescence reference slides and observing the profile in the detector. The focal-length of $f = \infty$ indicates parallel beam, whereas diverging and converging beams correspond to negative and positive focal-lengths. The field of view at the working distance of the objective is minimum at $f = \infty$ (for parallel beam) and increases for smaller ATL focal-lengths. A change in the direction of current results in proportional change in FOV on the left side of $f = \infty$ [see Fig. 2(a)]. The near-linear nature of FOV over the focal length $-500\,\text{mm} \leq f \leq \infty\,\&\,\infty \leq +200\,\text{mm}$ is quite evident. Figure 2(b) shows the variation in the ATL focus with the applied current that largely displays linear behavior. Figure 2(c) displays the corresponding FOV for the entire range of ATL focal lengths. Such a large variability is helpful for applications that require adaptive and rapid change of FOV.

Field homogeneity greatly improves image quality. Specifically, homogeneity is desired for understanding protein dynamics/protein migration or cell physiology based on its local distribution. To demonstrate this, we carried out surface plot of log-PSF, as shown in Fig. 3(a). Near flat-top of the PSF cross section at the working distance of objective lens visually ensures homogeneity over a large FOV. Figure 3(b) displays the corresponding intensity-plot along a line passing through the center of log-PSF (see the inset). The slow variation of intensity on either side of the center gives an indication of field homogeneity when compared to $f = \infty$. It is evident that adaptive change of FOV leads to field homogeneity.

To demonstrate the technique, we have imaged Dendra2-HA transfected NIH3T3 cells following established protocol.[1] The process begins with thawing the cells and culturing them for two passages. The cells were cultured with a complete growth media (80% DMEM + 10% calf bovine serum + 4.5 ml penicillin streptomycin) on glass coverslip in a 35 mm cell-culture disk. A cell density of $10^5/\text{cm}^2$ is targeted, and a confluency of 80% is ensured. NIH3T3 mouse fibroblast cells were transiently transfected with plasmid Dendra2-Hemagluttinin (Dendra2-HA) (photoactivable probe). Then, the cells were cleaned with phosphate-buffer saline (PBS) few times

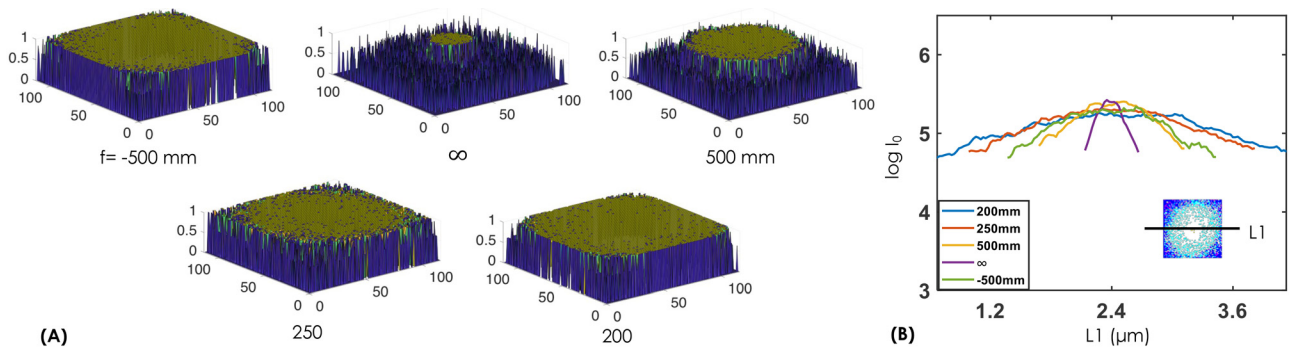

FIG. 3. (a) The field homogeneity over FOVs displayed using surface plots of log-PSFs. (b) The corresponding intensity across the spot (log-PSFs) along line (L1) shows the rapidity of the fall of intensity within FOV as compared to $f = \infty$.

and fixed with 4% PFA, and sealed with another glass slide using fluorosave solvent. We inspect the cells before and after the fixation process with PFA and follow established protocol for NIH3T3 cells.[5,7,49] Moreover, we did not notice substantial changes, which is also supported by the fact that PFA-based chemical fixation of cultured cells is better than conventional treatment methods.[5,49] The transfected cells were then recognized by observing green fluorescence (at a wavelength of 507 nm) from it when illuminating by a blue light source (470–490 nm) integrated with the Olympus IX81 microscope (not shown in Fig. 1). Subsequently, the cells were imaged using the developed aSMLM super-resolution microscope. The laser power used for activation and excitation of photoactivable probe was 112 μW and 6.3 mW, respectively. A total of 5000 images were acquired at an exposure time of 33 ms, and approximately 25 000 molecules were recorded by the EMCCD camera (iXon Ultra 897, Andor Tech., UK). Background subtraction and particle filtering were carried out to remove background and minimize false counting. This is followed by extracting spots and fitting them with a 2D Gaussian function. Subsequently, the centroid and localization precision ($\Delta_{lp} \approx \Delta_{psf}/\sqrt{N}$, where Δ_{psf} and N are diffraction-limited PSF and detected photons, respectively) were determined.

Figure 4 shows the reconstructed image of single molecule in a cell section. Imaging is performed at variable FOV, and the corresponding reconstructed single molecule image is shown along with a zoomed section. The transfected image of the cell is also shown along with a red circle that visually marks approximate FOV. The corresponding intensity along a radial line (red line L1) determines the change in intensity across FOV (see red dotted circle). The sharp fall of intensity at $f = +250$ mm and $f = +200$ mm when compared to $f = \infty$ is quite evident that clearly separates the FOV from background (see associate intensity plots). Note that $f = \infty$ generates parallel beam that turns our system into a traditional SMLM. Moreover, a larger FOV at $f = +200$ mm is quite evident when compared to $f = \infty$. Thus, aSMLM enables imaging of a relatively large specimen area when compared to traditional SMLM. Subsequently, the average number of molecules is estimated as shown in Fig. 5. The insets show corresponding localization-plots at varying ATL focal lengths (-500 to $+200$ mm). A substantial increase (approximately threefold) is noted in the recorded number of molecules at $f = +200$ mm when compared to $f = \infty$. This directly correlates the number of detected single molecules and the system FOV.

As an application, we investigated the clustering process in the Influenza A disease model that involves the distribution and assembly of Hemagglutinin (HA) protein in NIH3T3 cells. Clustering is a key process that determines Hemagglutinin dynamics inside the cell beginning from entry to its maturation during infection. The viral glycoproteins of hemagglutinin (HA) are localized in the plasma membrane of the host cell in clusters and are utilized by virus for fusion, viral budding, and infection.[5,43–46] A high density of HA on the resultant virions is essential for its entry and subsequent fusion with the next host cell. HA facilitates viral entry through fusion pore in the host endosomal membrane, which leads to the delivery of viral RNA into the cytoplasm.[44,48] The distribution of HA and its assembly in the plasma membrane depend on raft microdomains (selective concentrated devices for protein complexes) for budding and fusion.[43,47] Overall, HA strongly associates with lipid rafts and clusters there to mediate strong virus-cell fusion. The sample preparation and related details are

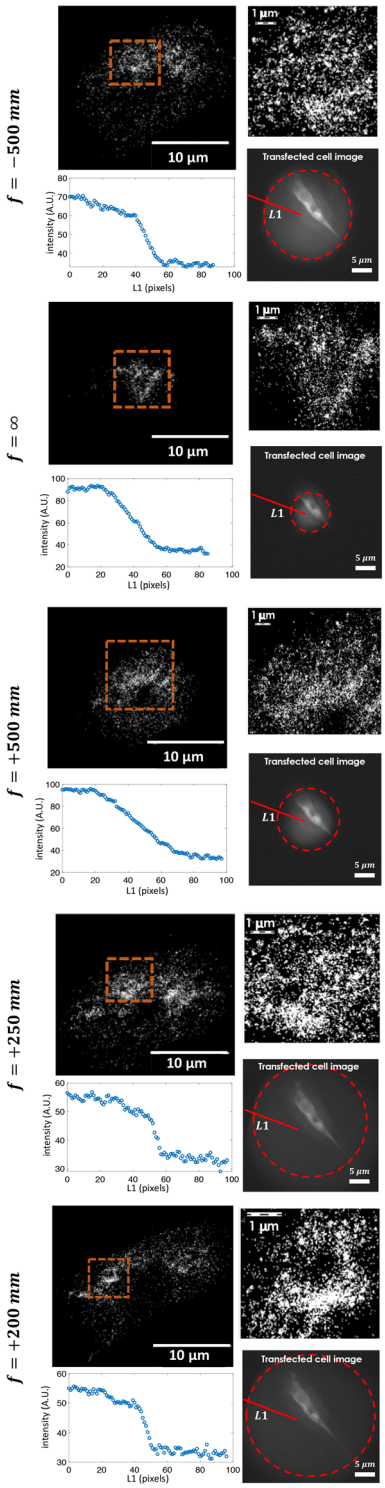

FIG. 4. Reconstructed single molecule image at varying focus of ATL ($f = -500$ mm, $\infty + 500, +250, +200$ mm). The insets show enlarged section of single molecules and the FOV (shown by red circle) along with intensity variations along L1.

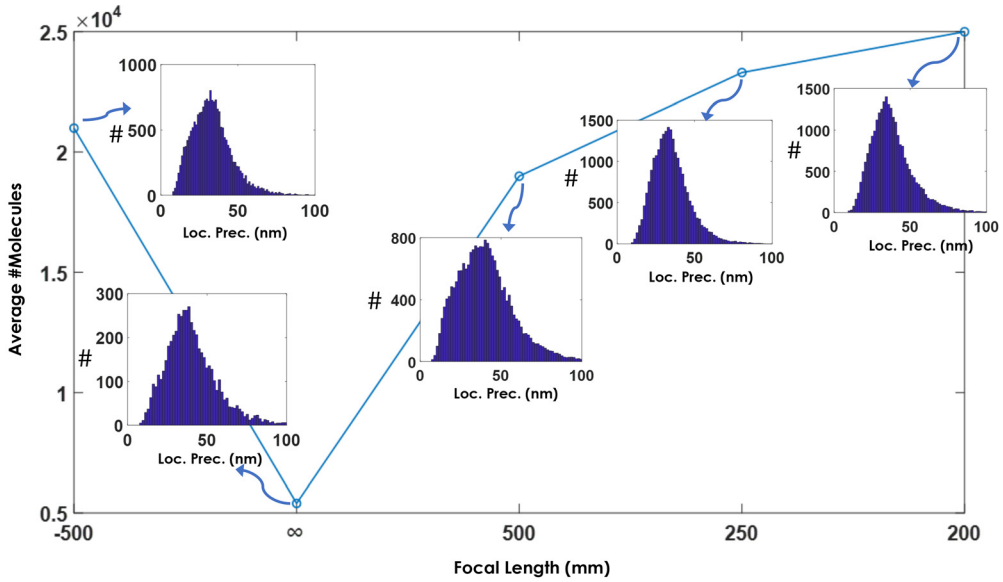

FIG. 5. The total number of detected molecules in the FOV at varying ATL focal-lengths. The corresponding localization precisions are also displayed. An increase in the number of molecules is evident.

adapted from Ref. 1.[7] The point-clustering method is used to identify HA clusters. Figure 6 shows clustering of HA molecules at different FOVs along with the transmission image of the cell. It is immediately evident that the technique allows visualization of clusters over a large FOVs ranging from 14.79 to 316.31 μm^2. This ensures that the technique allows large-scale study of HA molecules and their behavior (migration, accumulation, and distribution) over time. The inset shows estimated critical biophysical parameters, such as cluster density, cluster area, and # molecules per cluster. These parameters are critical for investigating membrane organization and accessing its role in viral infection. For example, the concentration of HA along with its clusters size and density in the host cell membrane is crucial for the release of bud-particles from infected cells.[50,51] Thus, there is a strong need to understand these clusters (size range, composition, and its

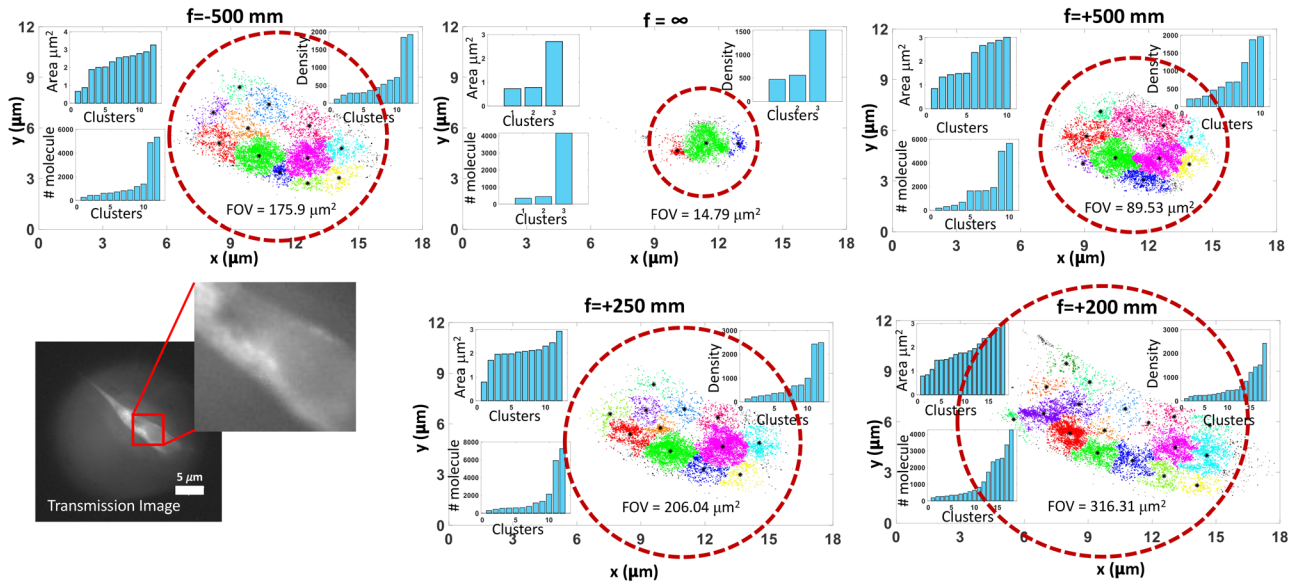

FIG. 6. Clustering of single molecules using the point-clustering method at varying ATL focal-lengths or equivalently at varying system FOV. The inset plots correspond to cluster density, cluster size (area), and number of molecules per cluster. Alongside transmission image is also shown.

dynamics) overtime in cells. The ability to investigate single molecule clustering at a desired FOV adds a new dimension to single molecule imaging and expands the reach of SMLM.

In conclusion, we have proposed a technique for adaptively varying FOV for traditional SMLM. This is achieved using an auto-tunable 4*f* sub-system that enables variable FOV imaging. The field, thus, generated at the geometrical focus shows better homogeneity over a large area (few tens to hundreds of square micrometer). The study on single-molecule (Dendra2-HA) aggregates in the transfected NIH3T3 cells, and the determination of critical biophysical parameters indicates the potential of aSMLM for extensive FOV investigation. Single-molecule studies show variable FOV investigation with the benefit of near-uniform illumination, better homogeneity, and easy integration with available SMLMs. We anticipate that the proposed technique may facilitate application in neurobiology and applied biophysics for understanding interaction over variable FOV with the resolution of single-molecule.

The authors acknowledge financial support from parent institute (Indian Institute of Science, Bangalore, India).

AUTHOR DECLARATIONS

Conflict of Interest

The authors have no conflicts to disclose.

DATA AVAILABILITY

The data that support the findings of this study are available from the corresponding author upon reasonable request.

REFERENCES

[1]P. P. Mondal, PLoS One **15**, e0242452 (2020).
[2]S. Schnorrenberg, T. Grotjohann, G. Vorbrüggen *et al.*, eLife **5**, e15567 (2016).
[3]B. Dong, X. Yang, S. Zhu, D. C. Bassham *et al.*, Sci. Rep. **5**, 15694 (2015).
[4]J. Liesche, I. Ziomkiewicz, and A. Schulz, BMC Plant Biol. **13**, 226 (2013).
[5]S. T. Hess, T. J. Gould, M. V. Gudheti *et al.*, Proc. Natl. Acad. Sci. **104**, 17370–17375 (2007).
[6]M. V. Gudheti, N. M. Curthoys, T. J. Gould *et al.*, Biophys. J. **104**, 2182–2192 (2013).
[7]N. M. Curthoys, M. J. Mlodzianoski, M. Parent *et al.*, Biophys J. **116**, 893–909 (2019).
[8]H. Colin-York, Y. Javanmardi, M. Skamrahl *et al.*, Cell Rep. **26**, 3369–3379 (2019).
[9]M. Fritzsche, R. A. Fernandes, V. T. Chang *et al.*, Sci. Adv. **3**, e1603032 (2017).
[10]S. W. Hell and J. Wichmann, Opt. Lett. **19**, 780–782 (1994).
[11]S. T. Hess, T. P. K. Girirajan, and M. D. Mason, Biophys. J. **91**, 4258–4272 (2006).
[12]M. J. Rust, M. Bates, and X. Zhuang, Nat. Methods **3**, 793 (2006).
[13]E. Betzig, G. H. Patterson, R. Sougrat *et al.*, Science **313**, 1642–1645 (2006).
[14]M. G. Gustafsson, Proc. Natl. Acad. Sci. U. S. A. **102**, 13081 (2005).
[15]J. Fölling, M. Bossi, H. Bock *et al.*, Nat. Methods **5**, 943 (2008).
[16]T. Dertinger, R. Colyer, G. Iyer *et al.*, Proc. Natl. Acad. Sci. U. S. A. **106**, 22287 (2009).
[17]A. Sharonov and R. M. Hochstrasser, Proc. Natl. Acad. Sci. U. S. A. **103**, 18911–18916 (2006).
[18]G. Giannone, E. Hosy, F. Levet *et al.*, Biophys. J. **99**, 1303–1310 (2010).
[19]P. P. Mondal, Microsc. Res. Tech. **80**, 333 (2017).
[20]P. P. Mondal and S. T. Hess, Appl. Phys. Lett. **110**, 211102 (2017).
[21]K. C. Gwosch, J. K. Pape, F. Balzarotti *et al.*, Nat. Methods **17**, 217–224 (2020).
[22]Y. Zhang, L. K. Schroeder, M. D. Lessard *et al.*, Nat. Methods **17**, 225–231 (2020).
[23]K. AbuZineh, L. I. Joudeh, B. A. Alwan *et al.*, Sci. Adv. **4**, eaat5304 (2018).
[24]M. J. Mlodzianoski, iSci. Note. **1**, 1 (2016).
[25]J. V. Thevathasan, M. Kahnwald, K. Cieśliński *et al.*, Nat. Methods **16**, 1045–1053 (2019).
[26]S. Habuchi, iSci. Note. **4**, 1 (2019).
[27]H. Ma, J. Xu, and Y. Liu, Sci. Adv. **5**, eaaw0683 (2019).
[28]R. Turcotte, Y. Liang, M. Tanimoto *et al.*, Proc. Natl. Acad. Sci. **116**, 9586 (2019).
[29]M. Valles and S. T. Hess, iSci. Note. **2**, 1 (2017).
[30]C. Wang, M. Taki, Y. Sato *et al.*, Proc. Natl. Acad. Sci. **116**, 15817 (2019).
[31]M. Weigert, U. Schmidt, T. Boothe *et al.*, Nat. Methods **15**, 1090–1097 (2018).
[32]C. Belthangady and L. A. Royer, Nat. Methods **16**, 1215–1225 (2019).
[33]H. Wang, Y. Rivenson, Y. Jin *et al.*, Nat. Methods **16**, 103–110 (2019).
[34]C. Qiao, D. Li, Y. Guo *et al.*, Nat. Methods **18**, 194–202 (2021).
[35]A. Pan, C. Zuo, and B. Yao, Rep. Prog. Phys. **83**, 096101 (2020).
[36]I. Kernier, A. Ali-Cherif, N. Rongeat *et al.*, J. Biomed. Opt. **24**, 1 (2019).
[37]Z. Zhao, B. Xin, L. Li *et al.*, Opt. Express **25**, 13382–13395 (2017).
[38]S. Pacheco, C. Wang, M. K. Chawla *et al.*, Sci. Rep. **7**, 13349 (2017).
[39]W. Hwang, J. Seo, DEun Kim *et al.*, Commun. Biol. **4**, 91 (2021).
[40]O. Helle, Opt. Express **27**, 6700–6710 (2019).
[41]B. Schreiber, Opt. Lett. **42**, 3880–3883 (2017).
[42]K. Ellefsen, PLoS One **10**, e0136055 (2015).
[43]S. Manes S, G. del Real, and C. Martinez, Nat. Rev. Immunol. **3**, 557–568 (2003).
[44]D. C. Wiley and J. J. Skehel, Annu. Rev. Biochem. **56**, 365–394 (1987).
[45]S. T. Hess, M. Kumar, A. Verma *et al.*, J. Cell Biol. **169**, 965–976 (2005).
[46]R. W. Ruigrok, P. C. Krijgsman, F. M. de Ronde-Verloop *et al.*, Virus Res **3**, 69–76 (1985).
[47]K. Simons and E. Ikonen, Nature **387**, 569–572 (1997).
[48]J. White, A. Helenius, and M. J. Gething, Nature **300**, 658–659 (1982).
[49]Y. Zhou, H. Mao, B. Joddar *et al.*, Sci. Rep. **5**, 11386 (2015).
[50]B. J. Chen, G. P. Leser, and R. A. Lamb, J. Virol. **81**, 7111–7123 (2007).
[51]M. Takeda, G. P. Leser, and R. A. Lamb, Proc. Natl. Acad. Sci. U. S. A. **100**, 14610–14617 (2003).